Reactions of Ruthenium Cyclopentadienyl Praecursor in the Metal Precursor Pulse of Ru Atomic Layer Deposition

Ji Liu[a], Hongliang Lu[b], David Wei Zhang[b], and Michael Nolan[a,c*]

[a] Tyndall National Institute, University College Cork, Lee Maltings, Dyke Parade, Cork, T12 R5CP, Ireland

[b] State Key Laboratory of ASIC and System, Shanghai Institute of Intelligent Electronics & Systems, School of Microelectronics, Fudan University, Shanghai 200433, China

[c] Nanotechnology and Integrated Bioengineering Centre, Ulster University, Shore Road, Co Antrim, BT37 OQB, Northern Ireland

Corresponding author:

[*]E-mail: Michael.nolan@tyndall.ie. Tel: +353 021 2346983

Abstract

Ruthenium is a promising material in the semiconductor industry and is investigated as the interconnect metal or as a seed layer for Cu interconnects. Non-oxidative reactants are required in a plasma-enhanced atomic layer deposition (PE-ALD) process for metals to avoid oxygen contamination. The PE-ALD of Ru has been explored experimentally, but the growth mechanism is not clear. In this paper, the reaction mechanism of the cyclopentadienyl (Cp, C_5H_5) precursor $RuCp_2$ and NH_x-terminated Ru surfaces that result from the plasma cycle is studied in detail by first-principle calculations. The Cp ligands are eliminated by hydrogen transfer and desorb from metal surface as CpH. The results show that on the NH_x-terminated Ru surface at typical ALD operating condition (temperature range 550K to 650K), the first hydrogen transfer is the rate-limiting step and has high barriers, which are -1.51eV for Ru(001) and 2.01eV for Ru(100). Assuming that the initial activation barrier for the first hydrogen transfer can be overcome, the two Cp ligands will be completely eliminated completely on Ru(100) surface during the metal precursor pulse, resulting in Ru atoms on the surface, binding to N atom. But at most only one Cp ligand is eliminated on Ru(001) surface, resulting in an RuCp termination on (001) surface. Investigating the precursor coverage, the final surface coverages of final terminations after the metal precursor pulse are 0.85 RuCp/nm^2 on the NH_x-terminated Ru(001) surface and 2.02 Ru/nm^2 on the NH_x-terminated Ru(100) surface. However, if the first H transfer barrier cannot be overcome, leaving $RuCp_2$ on NH_x-terminated Ru surfaces, the maximum coverages of $RuCp_2$ on Ru(001) and Ru(100) surfaces are 2.54 $RuCp_2$/nm^2 and 2.02 $RuCp_2$/nm^2. These structures are vital to model the following N-plasma step.

1. *Introduction*

Ruthenium (Ru) thin film is a widely studied material in the semiconductor industry due to its excellent electrical properties and chemical stability.[1] As the downsizing of semiconductor devices continues, the widely used copper interconnect is coming up against critical issues including diffusion into the substrate dielectric layer and the difficulty to deposit continuous films in ever reducing via volumes.[2] Due to its low resistivity and high chemical stability, Ru is a leading candidates in replacing Cu for interconnects and has been applied as metallization in interconnects or a seed layer for copper interconnects.[3-5] In addition, Ru can be applied in other device applications, including the gate metal for semiconductor transistors and the electrode material in dynamic random access memory (DRAM) devices.[6]

For the deposition of metal thin films on the high aspect ratio structures typically present in nanoscale devices, atomic layer deposition (ALD) is the only approach that allows conformal deposition and control of growth at the atomic level.[7-8] Generally, ALD consists of a self-limiting half cycle for each precursor, where the reactions will in principal finish after all available surface sites are consumed. This drives the self-limiting nature of ALD which enables the high level of growth control.

The study of Ru ALD has used Cp based precursors, $RuCp_2$ or $Ru(EtCp)_2$, and O_2.[9-10] O_2 is consumed with the hydrocarbon ligand of metal precursor. The reported primary by-products are CO_2 and H_2O.[11] The obtained Ru films then have oxygen impurities. This approach has been extended to deposit noble metals such as Pd and Pt [references]. The surface metal oxides are unstable and decompose to give metals at elevated temperatures.[12] For thermal ALD of Ru using dimethylbutadiene-based precursor $Ru(DMBD)(CO)_3$ and non-oxidative reactants hydrazine, the achieved growth rate is 0.42 Å /cycle with an ALD temperature window from 200 °C to 210 °C.[12]

In addition to thermal ALD, plasma-enhanced ALD (PE-ALD) has been used with ammonia or a mixture of N_2 and H_2 as the N-plasma source.[13-15] For the PE-ALD of Ru using $RuCp_2$ and NH_3 plasma at a temperature of 300 °C, a growth rate of 1.2 Å/cycle has been reported, while a growth rate of 1.8 Å/cycle was reported using $Ru(EtCp)_2$ at 300 °C.[16] Organometallic compounds such as β-diketonates have also been used as Ru precursors and the deposited Ru thin films show higher impurity concentration compared to using metallocenes such as $RuCp_2$ as the Ru precursor.[17]

Since oxygen can be involved in the deposition process, the quality of deposited Ru thin film depends strongly on the oxygen dose.[18-19] Obviously, oxygen can result in interfacial metal oxide formation through the oxide RuO_2.[18] To address this problem, non-oxidative reactants such as NH_3 or H_2 can be used to promote deposition of metal films.[20-23]

The deposited Ru thin film is crystalline with hexagonal structure. The orientation is random at low temperature. However, the [001] direction will dominate at elevated temperature or increased plasma power.[9, 24] Deposition of Ru on substrates including TaN, Si and SiO_2 with PE-ALD shows no nucleation delay in contrast to thermal Ru ALD.[16] One possible mechanism in PE-ALD is the production of highly reactive plasma radicals which can easily remove ligands and impurities. However, the detailed mechanism of plasma-enhanced ALD is still not known and requires further study of both the metal and the plasma steps.

Density functional theory (DFT) calculations have been successfully applied to study the ALD of metals and metal oxides.[25-28] There are some outstanding questions, including how to design new precursors with properties such as good volatility and high reactivity[29-30] or the reaction mechanism during the metal precursor pulse and plasma pulse. A reaction mechanism using oxidative reactants such as O_3 and H_2O has been elucidated.[31-35] However, when depositing metals, an O-source can promote oxidation of the metal and cause O-contamination. Non-oxidative

reactants such as NH_3 are used in the in PE-ALD of transition metals.[36] With this in mind, the key advance of the current paper is to determine the reactions that take place during the metal precursor pulse in Ru ALD which then serves as a foundation for the ongoing investigation of the atomic level mechanism of the plasma pulse, similar to our earlier work[37] on Co precursor reactions.

A complete PE-ALD process using N-plasma is as follows. After some cycles, the metal surface after the post-plasma stage is actually an NH_x-terminated metal surface, where *x* can be 1 or 2, NH or NH_2. In the first half-cycle, the metal precursor $RuCp_2$ will react with the NH_x-terminated metal surface. The Cp ligand is eliminated by hydrogen transfer to form CpH, which desorbs from surface. In the second half-cycle, the plasma generated radicals such as N_xH_y, N, or H will react with the precursor fragment-terminated metal surface and the Ru atoms are deposited on the surface, which is covered by NH_x groups at the end of second half cycle. In our recent published work, the nature and stability of NH_x-terminated metal surfaces were determined.[38] The results showed that at typical ALD operating conditions, a temperature range of 550K to 650K, on the Ru(001) surface, the most stable termination is NH-termination, while on the Ru(100) surface, a mixture of NH and NH_2 is the most stable surface termination.

In this paper, we explore the reaction mechanism for the metal precursor pulse on NH_x-terminated Ru (001) and (100) surfaces by DFT calculations. The metal precursor $RuCp_2$ reacts on these NH_x-terminated surfaces and the hydrogen transfer step is studied in detail with calculation of hydrogen migration barriers and the formation and elimination of CpH. Furthermore, we investigate the role of precursor coverage, aiming to determine the final precursor coverage and termination on Ru (001) and (100) surfaces. Assuming that the initial activation barrier for the first hydrogen transfer can be overcome, on the Ru(100) surface, the metal precursor can undergo two hydrogen transfer steps with elimination of the two Cp ligands. On the Ru (001) surface, we predict termination with

RuCp. The most favourable surface coverages of these precursor terminations are 0.85 RuCp/nm^2 on the NH_x-terminated Ru(001) surface and 2.02 Ru/nm^2 on the NH_x-terminated Ru(100) surface. However, if the process temperature would not permit the first H transfer barrier to be overcome, thus leaving $RuCp_2$ on the NH_x-terminated Ru surfaces, the maximum coverages of $RuCp_2$ on Ru(001) and Ru(100) surfaces are 2.54 $RuCp_2$/nm^2 and 2.02 $RuCp_2$/nm^2.

2. *Methods and Computational Details*

All the calculations are performed on the basis of spin-polarized DFT with the projector augmented wave (PAW) formalism, as implemented in the Vienna *ab* initio simulations package (VASP 5.4) code.[39] The generalized gradient approximation (GGA) with the parameterization of Perdrew-Burke-Ernzerhof (PBE) is used for the exchange-correlation functional.[40-41] The valence electrons are 8 for Ru, 5 for N, 4 for C, and 1 for H. The energy cutoff for the plane wave expansion is set to 400 eV. The convergence of energy and forces are set to 1×10^{-4} eV and 0.01eV/□, respectively. The bulk Ru crystal structure is optimized by simultaneously relaxing the ionic positions, cell volume and cell shape at a higher plane wave energy cutoff of 550eV and a Monkhorst-Pack grid k-point mesh[42] of 12 × 12 × 6. The resulting lattice constants are a = b = 2.71Å, and c = 4.28Å for Ru bulk.

The deposited Ru films by ALD are polycrystalline and have random surface orientations after low temperature deposition. Based on our previous study[38] on the stability of NH/NH_2 terminations, we have chosen the most stable (001) surface and the least stable, and high reactivity (100) surface, to investigate the precursor reaction mechanism. The (001) surface has smaller surface area than the (100) surface. Thus, a (4×4) supercell is used to simulate Ru(001) surface

while a (3×3) supercell is used to simulate Ru(100) surface. The calculated surface areas are 1.18nm^2 for Ru(001) and 0.99nm^2 for Ru(100). For (001) surface, a five-layer structure is built with the bottom three-layers fixed during the calculation; while for (100) surface, due to the unique zigzag structure, a four-bilayer (in total eight layers) structure is built with the bottom two-bilayer (bottom four layers) fixed during the calculations. From our previous studies, this is sufficient to model these Ru surfaces.[38]

A k-point mesh[42] of 2 × 2 × 1 is used in (4×4) supercell and that for the (3×3) supercell is 3 × 2 × 1. Our previous DFT study[38] of NH_x saturation coverage shows that at zero-K condition, where coverage is maximum, the Ru(001) surface is terminated with 1ML NH, which is modelled by 16 NH species in our (4×4) supercell. The termination on Ru(100) surface is 1ML NH and 1ML NH_2 due to the trench structure, which contains 9 NH and 9 NH_2 in our (3×3) supercell. NH prefers channel bridge site and NH_2 prefers surface bridge site. The configurations of single NH or NH_2 species adsorbed on preferred sites are shown in Figure S1 in supporting information. The saturation coverages are summarized in Table 1. The configurations of the NH_x-terminated Ru surfaces at maximum coverage are shown in Figure 1(a)-(b). The side view of these NH_x-terminated Ru surfaces is shown in Figure S2 of supporting information.

Table 1. The calculated saturation coverages on Ru (001) and (100) surfaces at zero-K (maximum coverages) and ALD conditions (low coverages).

	Ru (001) (4×4)	Ru (100) (3×3)
Zero-K condition	1ML NH	1ML NH + 1ML NH_2
ALD condition	0.89ML NH	0.67ML NH + 0.67ML NH_2

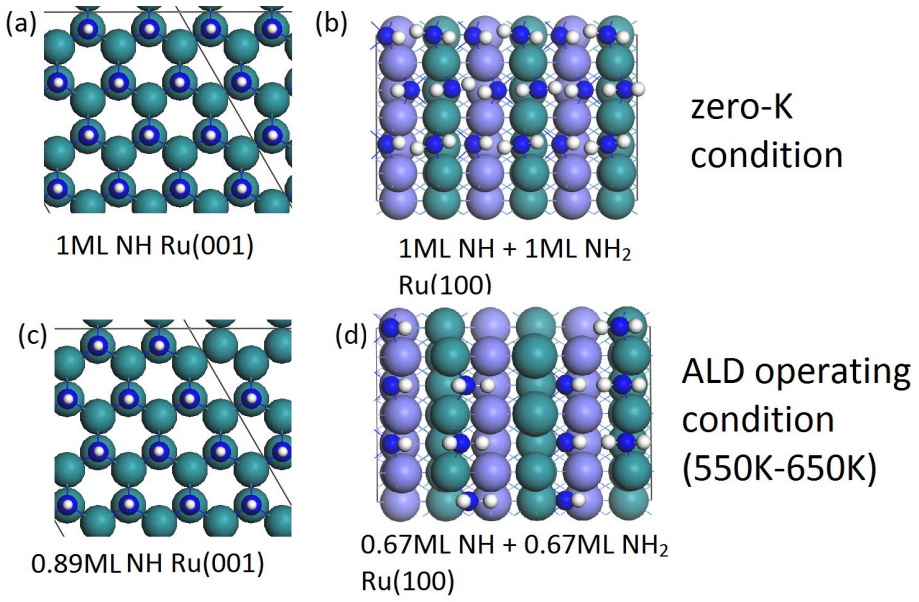

Figure 1. The top view of NH_x-terminated Ru surface at zero-K or high coverage condition including (a) Ru(001), and (b) Ru(100) and at ALD operating condition, with lower coverage including (c) Ru(001), and (d) Ru(100). Ru atoms are represented by green colour for surface terminating atoms and purple colour for the channel atoms in the (100) surface; N atom and H atom are represented by dark blue and white atom, respectively.

At the ALD operating condition (temperature range 550K to 650K), some of the surface NH_x species desorb from the surface. The NH_x saturation coverages are as follows: Ru(001) surface is terminated with 0.89ML NH, which is 14 NH in (4×4) supercell and the Ru(100) surface is terminated with 0.67ML NH and 0.67ML NH_2, which contains 6 NH and 6 NH_2 in (3×3) supercell. The configurations of NH_x-terminated Ru surfaces at the ALD operating condition are shown in Figure 1(c)-(d). On the (100) surface, due to the trench structure, NH prefers channel bridge site and NH_2 prefers surface bridge site.

The molecular geometry of the precursor $RuCp_2$ is relaxed in the same supercell as Ru(001) with the energy cutoff at 400eV and Gamma point sampling. The van der Waals correction is applied with PBE-D3 method to ensure an accurate description of the metal precursor adsorption energy.[43]

The activation barriers reported in this paper are computed using climbing image nudged elastic band (CI-NEB) method[44] with 6 images including the starting and ending geometries and with the forces converged to 0.05eV/Å.

3. *Results and Discussions*

3.1 Metal precursor adsorption on NH_x-terminated Ru (001) and (100) surfaces

For free metal precursor $RuCp_2$, the distance between the two Cp rings is 3.62Å and the Ru-C distance is 2.18Å. When adsorbed on the NH_x-terminated metal surfaces, the metal precursor can be placed perpendicular to substrate with one Cp ring interacting with the surface (which we term the **upright** adsorption mode) or parallel to surface with both Cp rings interacting with the surface (which we term the **horizontal** adsorption mode). An upright adsorption mode with one ring interacting with the surface and one ring pointing away from the surface has been reported for the adsorption of $FeCp_2$ on silica.[45] The adsorption energy is calculated from:

$$E_{ad} = E_{tot} - E_{\frac{NHx}{Metal}} - E_A \qquad (1)$$

where E_{tot}, $E_{NHx/Metal}$, and E_A are the energy of the NH_x-terminated metal slab with precursor $RuCp_2$, the slab model for the NH_x-terminated metal surface, and isolated precursor $RuCp_2$, respectively. A negative adsorption energy corresponds to exothermic adsorption. All the energies are computed with the van der Waals correction included. We will use the NH_x coverages obtained at zero K and ALD conditions to explore the effect of NH_x coverage on the $RuCp_2$ precursor pulse.

The calculated adsorption energies of $RuCp_2$ on NH_x-terminated Ru (001) and (100) surfaces at maximum NH_x coverages and low coverages are shown in Table 2. At maximum NH_x coverages,

Ru(001) is terminated with 1ML NH and Ru(100) has a mixed termination with 1ML NH and 1ML NH_2. On Ru(001) surface, the metal precursor prefers to bind to the substrate through only one Cp ring and the precursor is in the **upright** position; while on Ru(100) surface, the metal precursor prefers to bind to the substrate through both Cp rings and the precursor is in the **horizontal** configuration. These structures are shown in Figure 2(a)-(b).

At low NH_x coverage, the binding preference of the metal precursor at both surfaces is unchanged from the maximum NH_x coverages and these structures are shown in Figure 2(c)-(d). At low coverage, after adsorption on Ru(100) surface, one channel NH migrates to surface site. The configurations of less stable adsorption structures are shows in Figure S3.

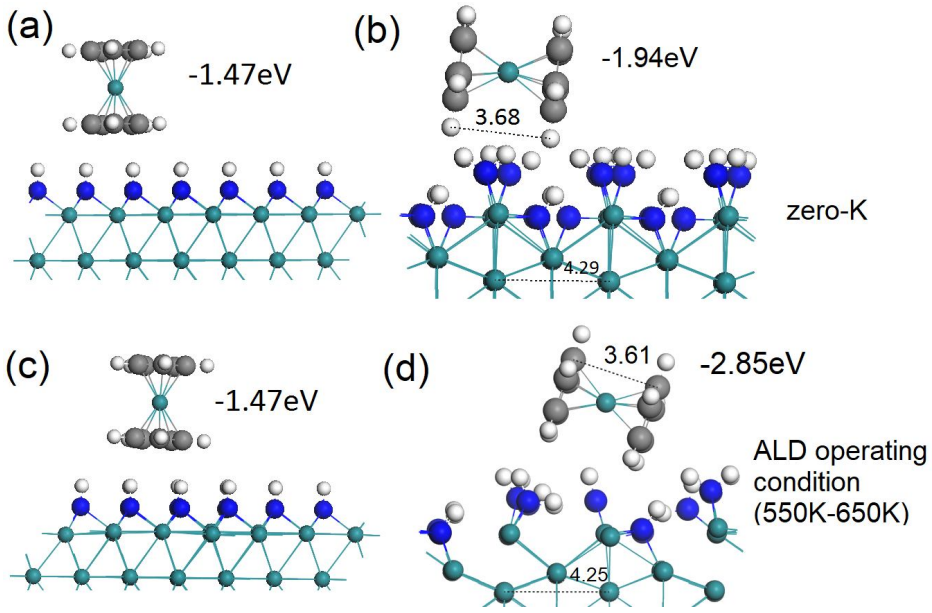

Figure 2. The configurations of the most stable adsorption mode of precursor $RuCp_2$ on (a) Ru(001) surface, and (b) Ru(100) surface at zero-K and on (c) Ru(001) surface, and (d) Ru(100) surface at ALD operating condition. Ru atoms are represented by green colour. N atom and H atom are represented by dark blue and white atom, respectively.

Table 2. The calculated adsorption energy of metal precursor $RuCp_2$ adsorbed on NH_x-terminated Ru (001) and (100) surfaces. The NH/NH_2 terminations include the maximum NH_x coverages at zero-K and low coverages at ALD operating condition (temperature range 550K - 650K).

	Maximum coverages		Low coverages	
	Ru(001)	Ru(100)	Ru(001)	Ru(100)
upright	-1.47	-0.77	-1.47	-0.57
horizontal	-1.28	-1.94	-0.61	-2.85

This difference in binding mode is due to the different surface structures. Ru(001) surface has a flat surface structure, while Ru(100) surface has a unique zigzag structure. On the Ru(001) surface, an upright position with one Cp ring close to metal surface can result in stronger adsorption strength. With this upright binding mode, each carbon atom in the Cp ring closest to the surface is potentially available for the hydrogen transfer step to form CpH.

At maximum coverages, the distances between the two Cp rings are in the range of 3.59Å to 3.63Å for $RuCp_2$ on Ru(001) surface. The distances for metal-C are in the range of 2.17Å and 2.19Å. Compared to free $RuCp_2$, the two Cp rings are slightly tilted. On Ru(100) surface, the distance across the trench (between two neighbouring metal atoms) is 4.29Å. The distances between the two Cp rings in precursors are in the range of 3.56Å to 3.68Å for $RuCp_2$ on Ru(100) surface. The two Cp rings are obviously tilted compared to adsorbed $RuCp_2$ on Ru(001) surface and free $RuCp_2$. The metal precursor can be well-accommodated within the trench of (100) surface, which can result in stronger adsorption strength.

At low coverages, the distances between the two Cp rings are in the range of 3.59Å to 3.64Å for $RuCp_2$ on Ru(001) surface. The distances for metal-C are between 2.17Å and 2.20Å. The NH_x coverages have little effect on the adsorption of $RuCp_2$ on (001) surface, for which the adsorption energy is -1.47eV. On the Ru(100) surface, the distance of the trench (two neighbouring metal atoms) is 4.25Å. The distances between the two Cp rings are in the range of 3.61Å to 3.65Å for $RuCp_2$ on Ru(100) surface. The distances for metal-C are between 2.18Å and 2.19Å. The adsorbed $RuCp_2$ on NH_x terminations at low coverages is less tilted compared to the maximum NH_x coverage. With this flat binding mode, the carbon atoms closest to the surface are available for hydrogen transfer to form CpH. We found a similar stability for $CoCp_2$ on NH_x-terminated Co (001) and (100) surfaces in earlier work[37], which suggests that the geometry of the surface plays a key role in the initial adsorption of the metal precursor.

3.2 Single precursor reaction pathway on Ru (001) and (100) surfaces with NH_x terminations at ALD operating condition

The reaction pathway during the metal precursor pulse is studied with respect to the NH_x terminations at ALD operating condition. In this section, we address the reaction mechanism when single $RuCp_2$ precursor is adsorbed on NH_x-terminated Ru (001) and (100) surfaces. Once the metal precursor is adsorbed on these NH_x-terminated metal surfaces, the Cp ligand can undergo hydrogen transfer, CpH formation, CpH desorption, second hydrogen transfer, and second CpH formation and desorption.

Upon adsorption, no spontaneous hydrogen transfer was observed on any NH_x-terminated Ru (001) and (100) surfaces. This means that the hydrogen transfer step must overcome an activation

barrier. The possible reactions of single adsorbed molecule of $RuCp_2$ on NH_x-terminated metal surfaces can be illustrated as follows:

$$A: H^* + RuCp_2 \rightarrow RuCp^* + HCp$$

$$B: H^* + RuCp \rightarrow Ru^* + HCp$$

where reaction A involves the first Cp ligand and reaction B involves the second Cp ligand. We have calculated the energy along the reaction pathway and the activation barriers for hydrogen transfer at each step. The reaction energies of precursor adsorption ($E_{adsorption}$), hydrogen transfer ($E_{hydrogen}^{I}$/ $E_{hydrogen}^{II}$) and CpH desorption ($E^{Des}{}_{CpH}^{I}$, $E^{Des}{}_{CpH}^{II}$) are with reference to the NH_x-terminated metal surface and free $RuCp_2$ as reactants and free CpH as a product.

The results for NH_x terminations at ALD operating condition are summarized in Figure 3 and the calculated barriers for the hydrogen transfer steps are presented in Table 3. In order to assess any role of NH/NH_2 coverage, the results for NH_x terminations at highest coverage, i.e. zero K, are summarized in Figure S4 and the calculated barrier for the hydrogen transfer steps are presented in Table S1 in supporting information.

Table 3. The calculated reaction energy for hydrogen transfer step and reaction barriers on Ru (001) and (100) surfaces with NH_x terminations corresponding to ALD operating condition. If the reaction energies of hydrogen transfer step are positive, the barriers are not calculated.

	$A: H^* + RuCp_2 \rightarrow RuCp^* + HCp$			$B: H^* + RuCp \rightarrow Ru^* + HCp$		
	$E_{adsorption}$	$E_{hydrogen}^{I}$	$E_{barrier}$	$E^{Des}{}_{CpH}^{I}$	$E_{hydrogen}^{II}$	$E_{barrier}$
Ru(001)	-1.47	0.03	1.51	0.71	1.44	Not Calculated
Ru(100)	-2.85	-1.44	2.01	-2.14	-1.68	1.00

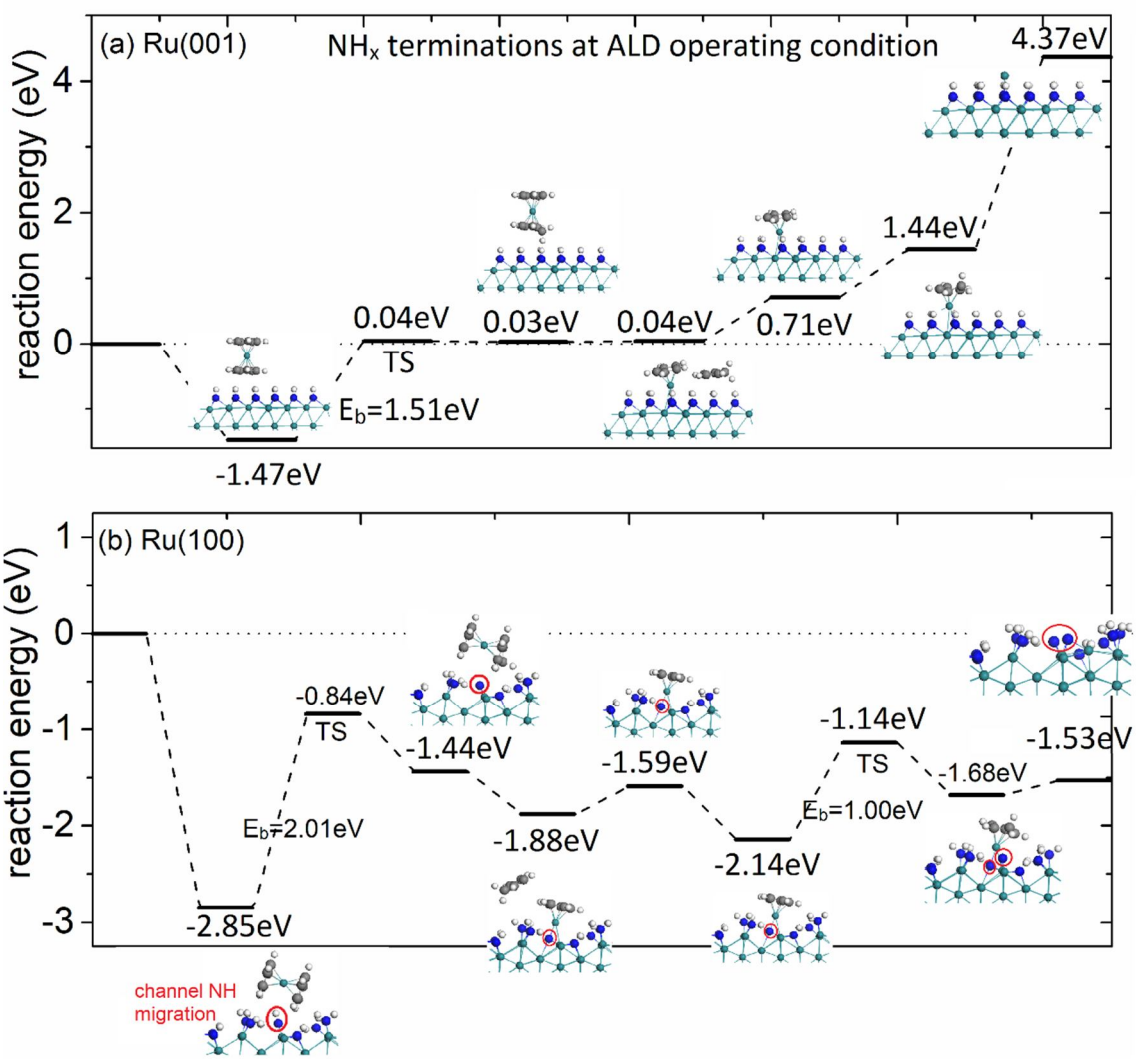

Figure 3. The plotted metal precursor reaction pathway on (a) Ru(001) surface and (b) Ru(100) surface with NH_x terminations at ALD operating condition. The Cp ligand is eliminated via hydrogen transfer. The substrate Ru atoms are represented by green spheres. Carbon, nitrogen and hydrogen atoms are represented by grey, blue and white colour, respectively. The red ring for Ru (100) highlights ….

At the Ru(001) surface, $RuCp_2$ has a strong adsorption strength with a negative adsorption energy of -1.47eV. The first hydrogen transfer step has a barrier of 1.51eV, while the first CpH desorption, to yield the RuCp surface termination, is endothermic by 0.71eV. Computing the energy for the

second CpH formation and desorption, we see that the reaction energy is as high as 4.37eV. Therefore, the final surface termination after introduction of single $RuCp_2$ precursor is possibly RuCp-terminated, assuming that the initial activation barrier for the first hydrogen transfer can be overcome.

At the highest NH_x coverage, the termination on Ru(001) is 1ML NH. As shown on Figure S4(a), the first hydrogen transfer has a barrier of 1.33eV. With the presence of adsorbed CpH, the second hydrogen transfer has a moderate barrier of 0.98eV. However, the energy cost of the desorption of the second CpH is as high as 2.92eV. This suggests a RuCp termination on the (001) facet irrespective of the NH_x coverage.

On the Ru(100) surface, we find that for the hydrogen transfer step, channel H atom is more reactive than surface H atom. As listed in Table 4, if the hydrogen transfer is from H atom of surface NH_2, after structure relaxing, surface N will grab the H atom from channel NH and revert to surface NH_2. Thus, in the discussion on Ru(100) surface, the channel H atom contributes to the hydrogen transfer. In addition, as shown in Figure 3(b), we found that for each hydrogen transfer step, the channel H migrates to a surface site and contributes to the hydrogen transfer.

On Ru(100) surface at ALD conditions, the favourable NH_x-termination is 6NH and $6NH_2$. The overall reaction of Cp ligand elimination via hydrogen transfer is exothermic. Upon adsorption, $RuCp_2$ has a high exothermic adsorption energy of -2.85eV. Due to the strong adsorption strength, the resulting first hydrogen transfer step has a high computed activation barrier of 2.01eV.

Table 4. The calculated reaction energy for hydrogen transfer step from surface H and channel H on Ru(100) surface. The results show that channel H is more reactive than surface H on Ru(100) surface.

	Zero-K condition	ALD condition
	Ru(100)/eV	Ru(100)/eV
adsorption	-1.94	-2.85
hydrogen transfer channel H	-0.79	-1.44
hydrogen transfer surface H	-0.05	revert to NH_2

After the first Cp ligand desorption, another channel NH migrates to surface site, ready to react with the second Cp ligand. The second hydrogen transfer reaction has a lower barrier of 1.00eV. Finally, after the second Cp ligand desorption, the energy gain is -1.53eV. This implies that upon adsorption of $RuCp_2$ on Ru(100) at 0.67ML NH and 0.67ML NH_2 terminations, two hydrogen transfer steps can take place, although whether this is possible is determined the process temperature, given the magnitude of the barrier for the first hydrogen transfer as a result of the extremely stable adsorption mode of the $RuCp_2$ precursor.

At the highest NH_x coverage, the termination on Ru(100) is 1ML NH + 1ML NH_2. As shown on Figure S4(b), the first hydrogen transfer has a high barrier of 2.72eV. At this maximum coverage, there are no available surface or channel sites. Thus, the migration of channel NH to surface site is not found. After the desorption of CpH, the second hydrogen transfer is not favoured due to positive reaction energy. This suggests a $RuCp_2H$ termination at maximum NH_x coverage, which

shows that the NH_x terminations can play a role in the activation barrier and reaction energy for Cp ligand elimination via hydrogen transfer.

In summary, for single metal precursor $RuCp_2$ on NH_x-terminated Ru (001) and (100) surface at ALD operating condition, the first hydrogen transfer is the rate-limiting step and the computed barriers are high for Ru (001) and (100) surface, which are 1.51eV for Ru(001) and 2.01 for Ru(100). Assuming that the initial activation barrier for the first hydrogen transfer can be overcome, on the Ru(001) surface, the second hydrogen transfer is not favoured due to positive reaction energy and endothermic reaction. The termination for a single $RuCp_2$ precursor on Ru(001) surface is RuCp fragment on the surface, binding to N atom. The distance between the Ru atom from RuCp fragment and nearest N atom is 1.88□.

On the Ru(100) surface, the barriers for the first and second hydrogen transfers are 2.01eV and 1.00eV. After the desorption of two CpH, the Ru atom is deposited on the surface with a negative energy gain of -1.53eV. The termination of single $RuCp_2$ precursor on Ru(100) surface is Ru atom, binding to N atom. The distance between the deposited Ru atom and nearest N atom is 1.89□. These structures are shown in Figure 4.

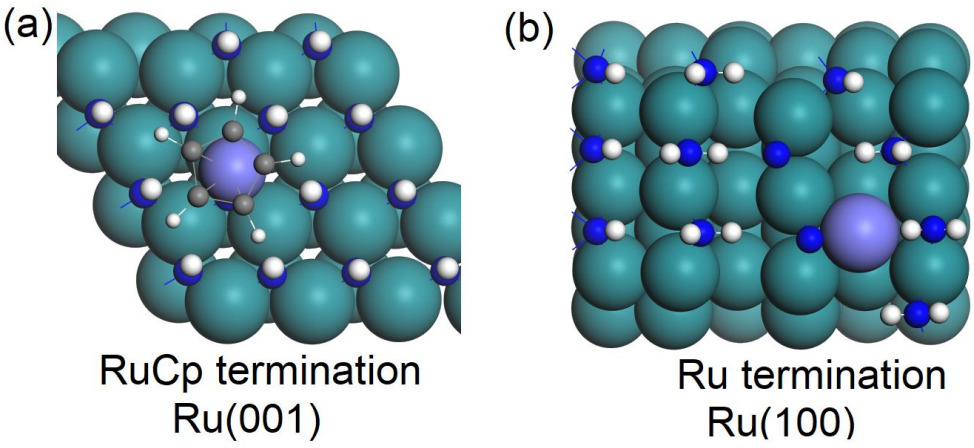

Figure 4. The structures of surface terminations for single $RuCp_2$ reaction on NH_x-terminated (a) Ru(001) surface and (b) Ru(100) surface. The substrate Ru atoms are represented by green spheres and Ru atoms from metal precursor are represented by purple spheres. Carbon, nitrogen and hydrogen atoms are represented by grey, blue and white colour, respectively.

3.3 Precursor coverage effect on the reaction mechanism on Ru (001) and (100) surfaces with NH_x terminations at ALD operating condition

We now address the adsorption and further reaction of two $Ru(Cp)_2$ precursors. The adsorption energy is calculated from:

$$E_{ad} = E_{tot} - E_{\frac{NHx}{Metal}} - 2 * E_A \qquad (2)$$

where E_{tot}, $E_{NHx/Metal}$, and E_A are the energy of the NH_x-terminated metal slab with two $Ru(Cp)_2$ precursors, the slab model for the NH_x-terminated metal surface, and free precursor $RuCp_2$, respectively. Dividing the computed energy by two gives the adsorption energy per precursor. All energies are computed with the inclusion of the van der Waals corrections. The adsorption structures of two precursors on Ru (001) and (100) surfaces at the ALD coverage of NH_x are shown in Figure 5.

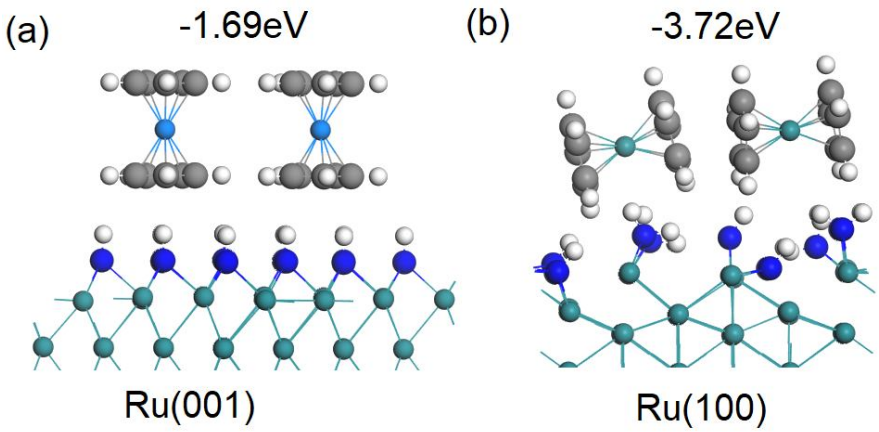

Figure 5. The configurations of two precursor Rup_2 on NH_x-terminated (a) Ru (001) surface, and (b) Ru(100). The substrate Ru atoms are represented by green spheres. Ru atoms from metal precursor $RuCp_2$ are presented by light blue spheres. Carbon, nitrogen and hydrogen atoms are represented by grey, blue and white colour, respectively.

The preferred binding mode for two precursors is the same as for adsorption of single precursor. On the Ru(001) surface, the **upright** adsorption mode is the most stable, while on the (100) surface the **horizontal** adsorption mode is the most stable. These energies of these adsorption modes are exothermic with computed adsorption energies of -1.69eV on the Ru(001) surface and -3.72eV on the Ru(100) surface, resulting in adsorption energies per precursor of -0.84eV on Ru(001) surface and -1.86eV on Ru(100) surface. Thus on both Ru (001) and (100) surfaces, while precursor adsorption is weaker compared with adsorption of single precursor (-1.47eV for Ru(001) and -2.85eV for Ru(100)), it is still exothermic and there is presumably some precursor-precursor interaction at this coverage in our surface supercell. Additionally, on the Ru(100) surface, after adsorption, one channel NH migrates to surface site, similar to our finding for single $RuCp_2$ adsorption on Ru(100) surface.

The further reaction of two precursor molecules of $RuCp_2$ on the NH_x-terminated metal surfaces at ALD operating condition can proceed as follows:

$$C\colon H^* + RuCp_2 + RuCp_2 \rightarrow RuCp_2 + RuCp^* + HCp$$

$$D1\colon H^* + RuCp_2 + RuCp^* \rightarrow RuCp_2 + Ru^* + HCp$$

$$D2\colon H^* + RuCp_2 + RuCp^* \rightarrow RuCp^* + RuCp^* + HCp$$

Here, after the first hydrogen transfer, Reaction C, the second hydrogen transfer can result in two different by-products. Reaction D1 results in an Ru atom and an intact adsorbed $RuCp_2$, while in reaction D2, two adsorbed RuCp fragments are present on the surface. The reaction energies of

two precursor adsorption are with reference to the NH_x-terminated metal surface and two free $RuCp_2$. If one CpH molecule desorbs from the surface, the reaction energies are with reference to NH_x-terminated metal surface, two free $RuCp_2$, and free CpH. The reaction pathways are shown in Figure 6, with Reactions D1 and D2 shown in different colours and the calculated barriers for each hydrogen transfer step are presented in Table 5.

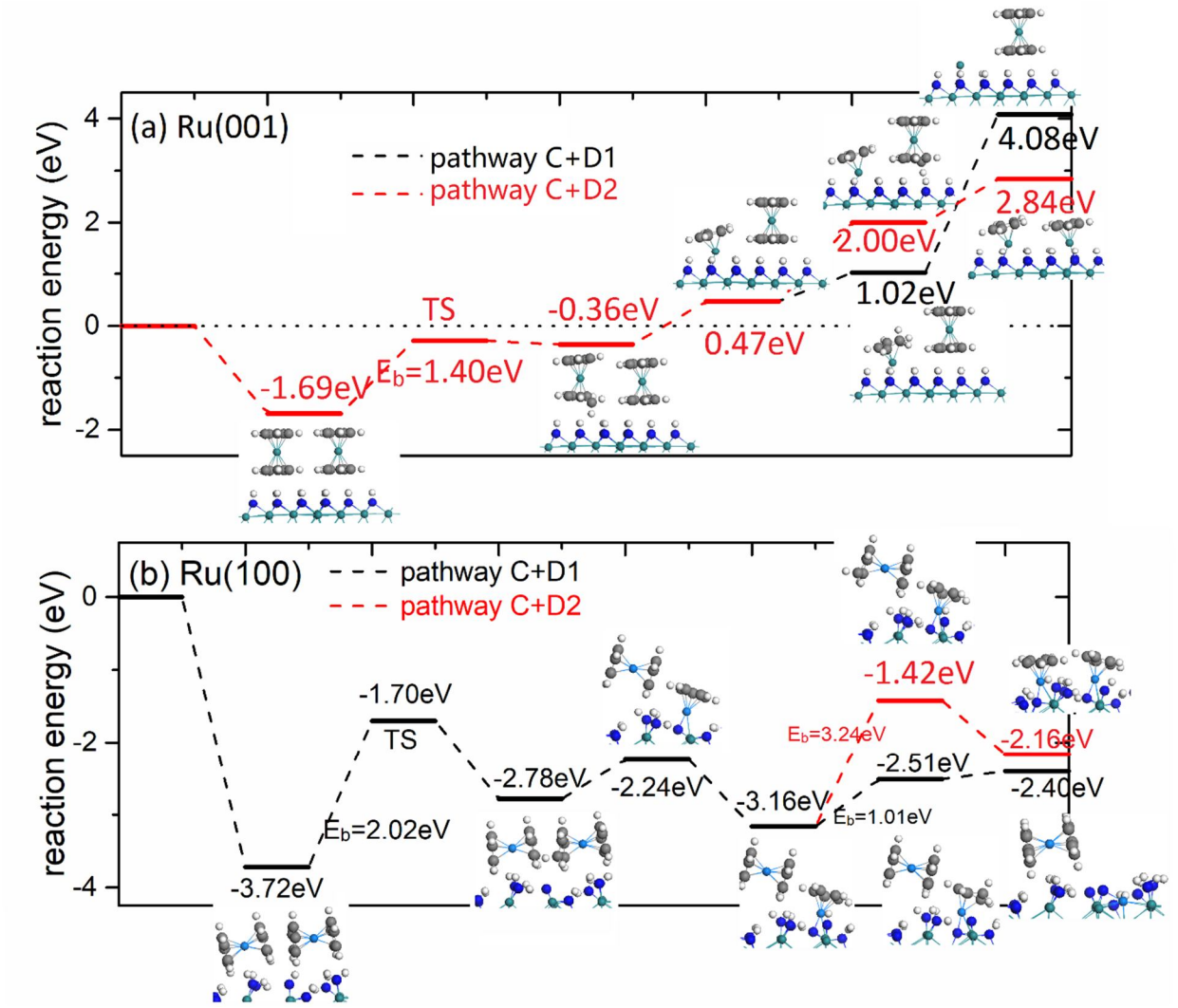

Figure 6. The $RuCp_2$ precursor reaction pathway on (a) Ru(001) surface and (b) Ru(100) surface for two $RuCp_2$ precursors. The black pathway is for reaction D1, resulting in a Ru atom and adsorbed $RuCp_2$. The red pathway is for reaction D2, resulting in two RuCp fragments at the surface. The Ru atoms are represented by green spheres. Carbon, nitrogen and hydrogen atoms are represented by grey, blue and white colour, respectively.

Table 5. The computed energy barriers for hydrogen transfer steps with respect to two metal precursors $RuCp_2$ adsorption on NH_x terminated Ru (001) and (100) surfaces at ALD conditions.

	Computed Barriers/eV		
	C: $H^* + RuCp_2 + RuCp_2 \rightarrow RuCp_2 + RuCp^* + HCp$	$D1$: $H^* + RuCp_2 + RuCp^* \rightarrow RuCp_2 + Ru^* + HCp$	$D2$: $H^* + RuCp_2 + RuCp^* \rightarrow RuCp^* + RuCp^* + HCp$
Ru(001)	1.40	Not calculated	Not calculated
Ru(100)	2.02	1.01	3.24

On Ru(001) surface, two $Ru(Cp)_2$ have a moderate adsorption energy of -1.69eV. The first hydrogen transfer step has a barrier of 1.40eV. Compared with single $RuCp_2$, this barrier is slightly reduced from 1.51eV. After CpH formation and desorption, the resulting adsorbed RuCp fragment and $RuCp_2$ has a positive reaction energy at the value of 0.47eV. The second hydrogen transfer via either pathway D1 or pathway D2 is not favoured. This implies that the surface coverage of $RuCp_2$ has little effect on Cp ligand elimination. With two $RuCp_2$ on Ru(001) surface, at most only one Cp ligand is eliminated.

On Ru(100) surface, the overall reaction of Cp ligand elimination via hydrogen transfer is exothermic. After adsorption of two $RuCp_2$, the channel NH migrates to surface site, resulting in strong adsorption energy of -3.72eV. The migration of channel NH to surface site is also observed for single $RuCp_2$ adsorption and Cp ligand elimination via hydrogen transfer. Due to this strong adsorption, the first hydrogen transfer has a high barrier at the value of 2.02eV. Compared with single $RuCp_2$, there is no difference in the barrier values. After the first CpH formation and desorption, another channel NH migrates to surface NH. For the second hydrogen transfer,

pathway D1 results in a Ru atom and $RuCp_2$ on the surface, and pathway D2 results in two RuCp fragments. The barrier analysis indicates that pathway D1 has a moderate barrier at the value of 1.01eV, but pathway D_2 has a high barrier of 3.24eV. Thus, on Ru(100) surface with two $RuCp_2$, the preferred surface termination is a deposited Ru atom binding to N atom and adsorbed $RuCp_2$.

On Ru(100) surface, after the elimination of two Cp ligands from the first $RuCp_2$ precursor, we then further investigate hydrogen transfer and Cp elimination for the second $RuCp_2$ precursor, with the deposited Ru on the Ru(100) surface. The reactions are illustrated as follows:

$$E: H^* + RuCp_2 + Ru^* \rightarrow RuCp^* + Ru^* + HCp$$

$$F: H^* + RuCp^* + Ru^* \rightarrow Ru^* + Ru^* + HCp$$

The results are summarized in Figure 7. Before the first hydrogen transfer, there is surface rearrangement via H_2 formation from one surface H and one channel H, which has an energy gain of -0.35eV. This is important for the elimination of surface NH_x species during the growth process. The first hydrogen transfer has a barrier of 1.67eV. After the first CpH formation and desorption, the second hydrogen transfer has a moderate barrier of 1.30eV. After the second CpH desorption, two Ru atoms are deposited on the surface, binding to N atom. The energy cost for the second CpH desorption is 1.62eV.

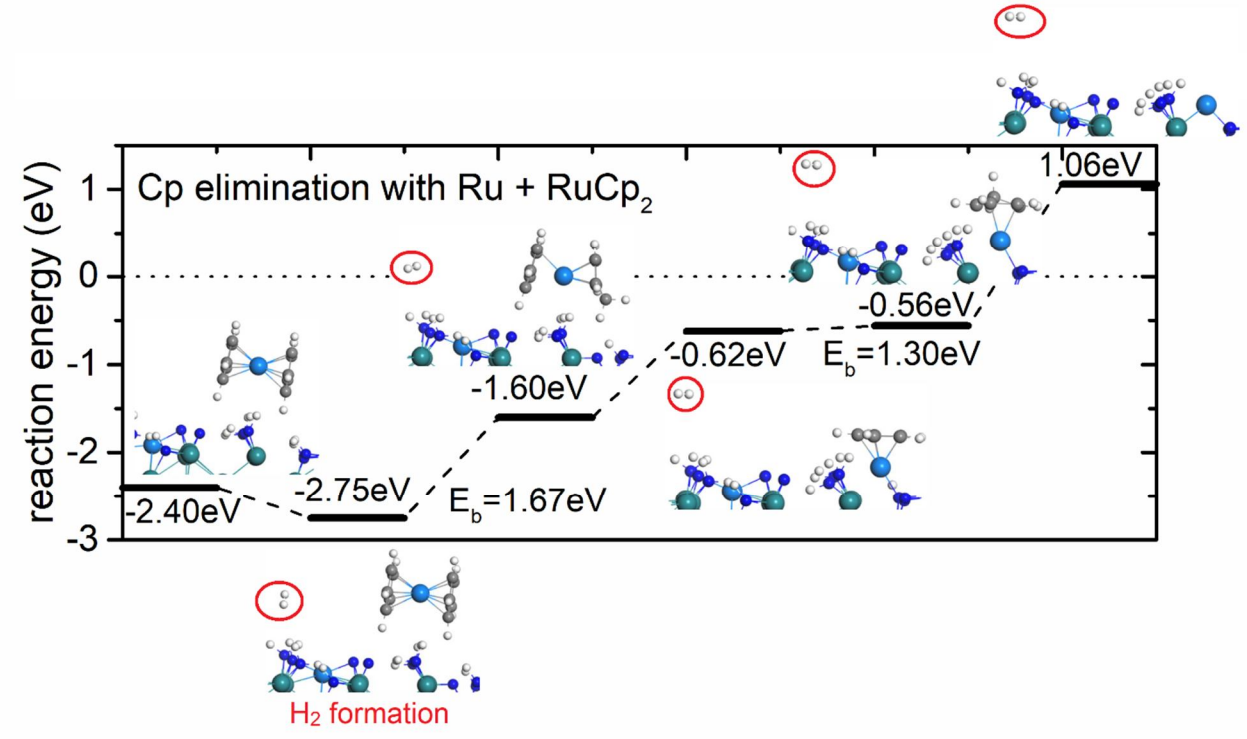

Figure 7. The plotted reaction pathway for Cp ligand elimination with one deposited Ru and $RuCp_2$ on Ru(100) surface. There is H_2 formation before hydrogen transfer step. The Ru atoms are represented by green spheres. Carbon, nitrogen and hydrogen atoms are represented by grey, blue and white colour, respectively.

The computed activation barriers for H transfer for single $RuCp_2$ precursor, two surface bound $RuCp_2$ species, and one precursor with a bare Ru atom Ru + $RuCp_2$ on Ru(100) surface are summarized in Table 6. We see that the activation barriers for Cp elimination via hydrogen transfer steps of single $RuCp_2$ and two $RuCp_2$ have no difference. For one precursor with bare Ru atom deposited on the surface Ru+$RuCp_2$, the barrier of first hydrogen transfer is reduced, but it is slightly increased for the second hydrogen transfer. The first hydrogen transfer is the rate-limiting step, which has higher activation barriers than the second hydrogen transfer. Assuming that the

initial activation barrier for the first hydrogen transfer can be overcome, the final structures can be determined.

Table 6. The calculated activation barriers for first and second hydrogen steps on NH_x-terminated Ru(100) surface with one precursor $RuCp_2$, two precursors $RuCp_2$ + $RuCp_2$, and one precursor and one Ru atom deposited on the surface Ru + $RuCp_2$.

	Barriers/eV		
	$RuCp_2$	$RuCp_2$ + $RuCp_2$	Ru + $RuCp_2$
1st hydrogen transfer	2.01	2.02	1.67
2nd hydrogen transfer	1.00	1.01	1.30

3.4 Final structures after metal precursor pulse on Ru (001) and (100) surfaces at ALD operating condition

On Ru(001) surface, the NH_x-termination is 14 NH at ALD operating condition. At most one Cp ligand is eliminated via hydrogen transfer, which depends on the condition that the activation barrier (1.51eV) can be overcome. With the presence of this RuCp fragment, any further Cp ligand via hydrogen transfer is not favoured due to positive reaction energy. At higher temperatures, the surface NH saturation coverage will be further reduced.[38] To examine this, we have calculated the reaction energy difference (ΔE) for the first hydrogen transfer step at different NH coverage on Ru(001) surface and these are summarized in Table 7.

On the Ru(001) surface, the zero-K surface termination is 1ML NH. If the temperature is increased to ALD operating condition (temperature range 550K to 650K), the surface termination will be

reduced to 0.89ML NH. Now, we continue decreasing the coverage and set the surface termination of Ru(001) at 0.50ML NH, 0.25ML NH and 0.06ML NH. The calculated reaction energy still remains positive for all coverages studied, and we can infer a continued high barrier for the first hydrogen transfer step, which is irrespective of the coverage of the NH surface termination. Thus, at most only one Cp ligand is eliminated, while the nature of the NH_x-termination has little effect on the elimination of the Cp ligand on Ru(001) surface. The final terminations after metal precursor pulse on Ru(001) surface at ALD operating condition is single RuCp fragment if the activation barrier for the first hydrogen transfer step can be overcome.

Table 7. The calculated reaction energy difference (ΔE) hydrogen transfer step on Ru(001) surface with various NH_x-terminations.

Ru(001)				ALD Temperature	Zero-K
	0.06ML NH	0.25ML NH	0.50ML NH	0.88ML NH	1ML NH
ΔE /eV	1.51	1.68	1.69	1.50	1.48

On the Ru(100) surface, the channel hydrogen atoms are involved in the hydrogen transfer steps and the two Cp ligands are eliminated via hydrogen transfer, CpH formation and desorption. At ALD operating condition, the NH_x-termination is 6 NH + 6 NH_2. There is H_2 formation during the Cp ligand elimination via hydrogen transfer. Thus, at most two Ru atoms are deposited on the surface, which depends on the condition that the high activation barrier (-2.01eV) for the first hydrogen transfer can be overcome.

The final structure on Ru(001) surface is RuCp fragment on the surface with the coverage of 0.85 RuCp/nm^2. The final structure on Ru(100) surface shows Ru atoms deposited on the surface with the coverage of 2.02 Ru/nm^2. These structures are shown in Figure 8.

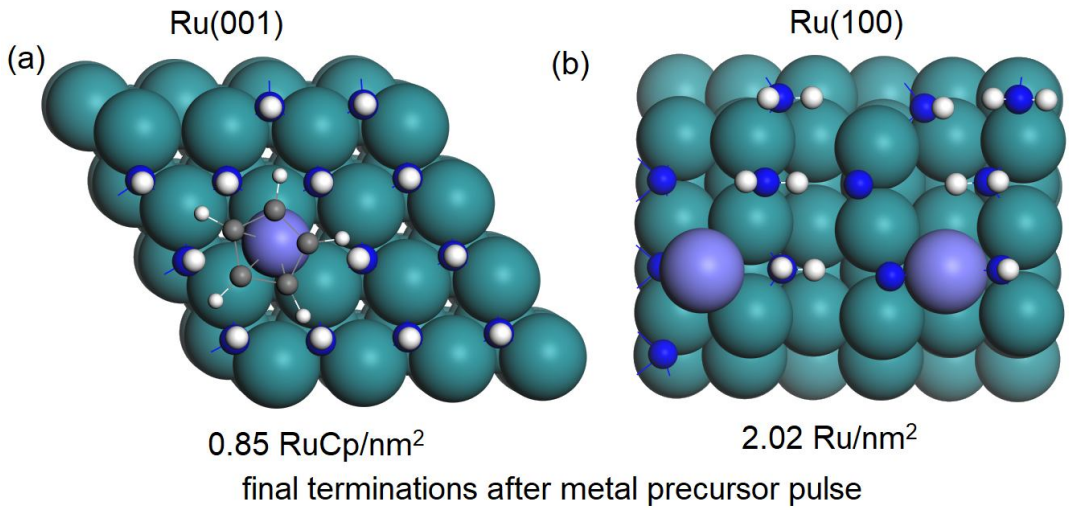

Figure 8. The configurations of final terminations after metal precursor pulse on Ru (001) and (100) surface. The substrate Ru atoms are represented by green spheres and Ru atoms from metal precursor are represented by purple spheres. Carbon, nitrogen and hydrogen atoms are represented by grey, blue and white colour, respectively.

4. Discussion

4.1 Effect of surface orientation on the deposition of Ru

The deposited Ru thin film is crystalline with hexagonal structure. The orientation is random at low temperature. However, the [001] direction will dominate at elevated temperature or increased plasma power.[9] Deposition of Ru on substrates including TaN, Si and SiO_2 with PE-ALD shows no nucleation delay in contrast to thermal Ru ALD.[16] $RuCp_2$ has been commonly used as Ru ALD

precursor experimentally. For the thermal ALD growth, the reported growth rate is 0.45 □/cycle with $RuCp_2$ and oxygen as the reactant.[46] PE-ALD can significantly reduce the incubation time.[13] The most commonly used precursor for PE-ALD of Ru is $Ru(EtCp)_2$. The reported growth rate varies from 0.16 □/cycle to 0.80 □/cycle, depending on the process condition such as reactor temperature (temperature range 100 °C to 300 °C) and plasma conditions (N_2/H_2 plasma and NH_3 plasma).[13] For example, Kwon et al. have reported a GPC at 0.38Å/cycle using $Ru(EtCp)_2$ and NH_3 plasma at 270 °C.[14] N_2/H_2 plasma can reduce the temperature to 200 °C and the GPC remains the same at 0.39 □/cycle.[47] The growth does not depend significantly on the plasma ambient given that there are NH_x species.

Theoretically, Phung *et al.*[26] have studied the deposition process of Ru on bare Ru surface with $RuCp_2$ and H_2 plasma. During the metal precursor pulse, $RuCp_2$ can perform dehydrogenation and ligand-dissociation process on bare Ru surface. They concluded that the growth on Ru(001) surface should be slow due to weak adsorption of $RuCp_2$. The surface terminations play an important role. They found that the presence of H on Ru surface after H plasma step can inhibit the growth of Ru. Thus, increasing the operating temperature can result in more available surface sites and increase the growth rate, which explains the experimental observed higher growth rate at elevated temperature.

In this study, we start with NH_x-terminated Ru surface[38] and the Cp ligand is eliminated via hydrogen transfer step. We see that the Cp ligand elimination via hydrogen transfer is endothermic and has high activation barriers on Ru(001) surface. The nature of the NH_x-termination has little effect on the elimination of the Cp ligand on Ru(001) surface. At most only one Cp ligand is eliminated, resulting RuCp fragment after metal precursor pulse at the coverage of 0.85 RuCp/nm^2. The growth of Ru on NH_x-terminated Ru(001) surface would be limited, which is similar to the

results of limited growth on bare Ru(001) surface from Phung's work[26] and would show a higher growth rate with temperature.

On Ru(100) surface, the two Cp ligands of $RuCp_2$ are eliminated completely, depending on the condition that the high activation barrier of the first hydrogen transfer can be overcome. Due to surface H_2 formation during the reaction, at most two Ru atoms are deposited on Ru(100) surface, resulting a final coverage of 2.02 Ru/nm^2. The orientation and surface termination of deposited Ru therefore impacts on the growth rate. This is one reason why the experimentally reported GPC varies with operating temperatures and Ru metal precursors.[13, 26]

From our previous theoretical study[37] on deposition of Co with $CoCp_2$, on Co(001) surface, a neighbouring $CoCp_2$ promotes the hydrogen transfer step by reducing the activation barriers. The overall computed activation barriers for Co are moderate. The final terminations are 3.03 CoCp/nm^2 on Co(001) surface and 3.33 Co/nm^2 on Co(100) surface. However, the ligand elimination on Ru(001) surface via hydrogen transfer is limited. We can predict that the orientation of deposited metals has moderate effect on the growth rate of Co, but the growth rate of Ru depends significantly on the orientation.

4.2 Reactions of the surface bound NH_x species on Ru(100) surface at the end of first half cycle

In the following N-plasma step, we expect any Cp ligands bound to Ru and surface NH_x species will be eliminated with plasma radicals N, H, NH and NH_2. The study of the plasma step is beyond the scope of this paper. However, we can explore some possible reactions of the surface bound NH_x species after CpH desorption on Ru(100) surface.

The structure of these surface bound NH_x species after CpH desorption on Ru(100) surface is shown in Figure 9(a). The channel NH_x species contain 5 bare N atoms and 1 NH species. The surface NH_x contains 5 NH_2 species and 1 NH species. The remaining channel H atom can form H_2 with one surface H atom and the relaxed structure is shown in Figure 9(b). Alternatively, the remaining channel H atom can transfer to surface site and the surface NH reverts to NH_2, which is shown in Figure 9(c). The calculated energy indicates that the H_2 formation and NH_2 formation are energetically favoured compared to surface bound NH_x species.

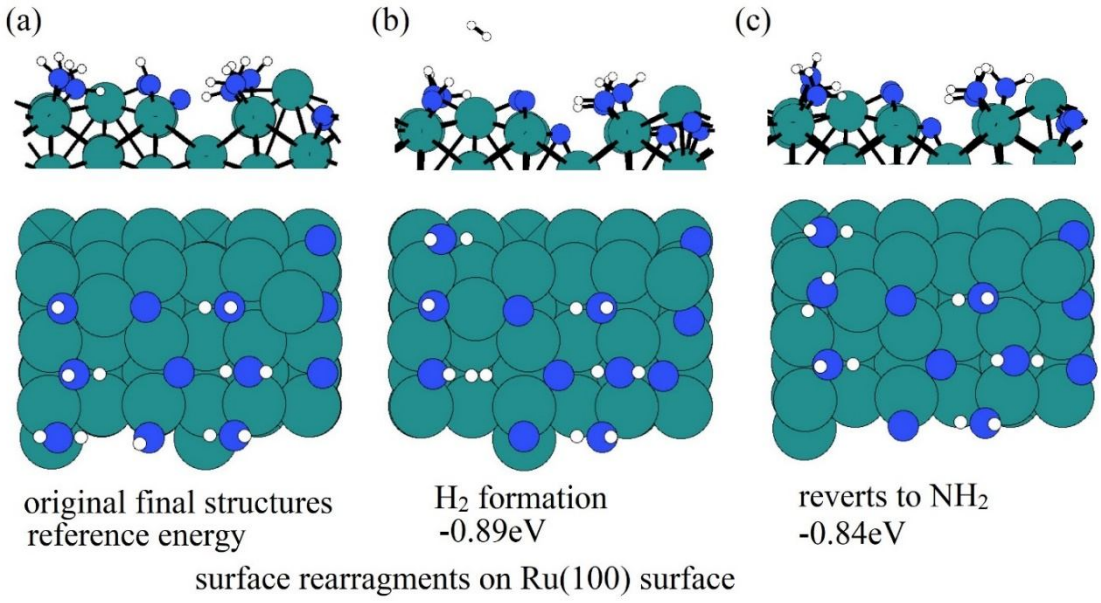

Figure 9. The configurations of surface reactions on the Ru(100) surface including (a) original final structure of Ru deposited on NH_x-terminated surface, (b) surface rearrangement via H_2 formation, and (c) surface rearrangement via reverting to NH_2. The substrate Ru atoms are represented by green spheres. Nitrogen and hydrogen atoms are represented by blue and white colour, respectively.

After the surface rearrangement, all the channel H atoms are consumed. We have further investigated the hydrogen transfer step with surface H atoms. The calculated reaction energies are listed in Table 8. The hydrogen transfer step has a positive reaction energy and is highly

endothermic. Thus, the surface H atoms are not involved in Cp ligand elimination via hydrogen transfer even if all the channel H atoms are consumed. These surface bound NH_2 species and channel N atoms will likely be removed in the following N-plasma step.

Table 8. The calculated reaction energies for Cp ligand elimination via surface H atoms on Ru(100) surface.

	reaction energy/eV	
	H_2 formation	NH_2 formation
$RuCp_2$ adsorption	-0.65	-0.73
Hydrogen transfer	1.40	1.47

4.3 Saturation coverages of $RuCp_2$ on Ru (001) and (100) surfaces

The discussion of final structures after metal precursor $RuCp_2$ pulse is based on the assumption that the high activation barriers of the first hydrogen transfer on Ru (001) and (100) surfaces can be overcome through the process temperature. This is due to the strong adsorption strength for $RuCp_2$ on NH_x-terminated Ru (001) and (100) surfaces. Thus, it is essential to determine the saturation coverages of $RuCp_2$ on these NH_x-terminated Ru surfaces.

In this study, a (4×4) supercell is used to simulate Ru(001) surface while a (3×3) supercell is used to simulate Ru(100) surface. The calculated surface areas are 1.18nm^2 for Ru(001) and 0.99nm^2 for Ru(100). At most four $RuCp_2$ can be placed on Ru (001) and (100) surfaces. The calculated

adsorption energies per precursor $RuCp_2$ are shown in Figure 10, which are all exothermic adsorption. These results are summarized on Table 9.

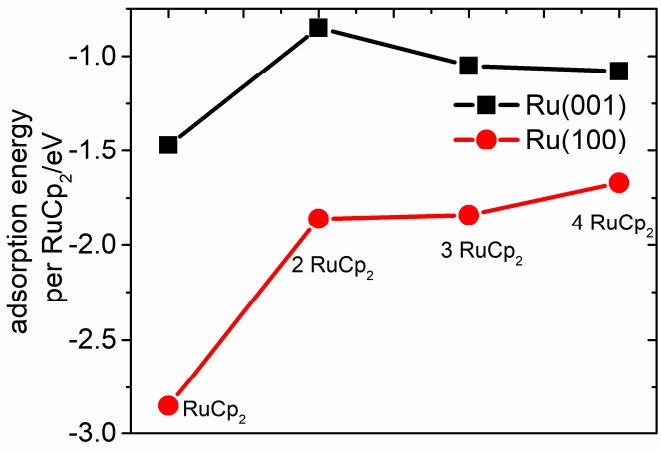

Figure 10. The plotted adsorption energies per $RuCp_2$ on NH_x-terminated Ru(001) and Ru(100) surfaces. The NH_x terminations are at ALD operating condition.

The binding energy difference (BE_{diff}) is computed by

$$BE_{diff} = E_{(n+1)RuCp2} - E_{nRuCp2} - E_A \qquad (3)$$

Table 9. The calculated adsorption energy per RuCp2 and binding energy difference (BE_{diff}) on Ru(001) and Ru(100) surfaces.

		$RuCp_2$	2 $RuCp_2$	23 $RuCp_2$	4 $RuCp_2$
Ru(001)					
	Ead/eV	-1.47	-0.85	-1.05	-1.08
	BE_{diff}/eV	-	-0.23	-1.47	-1.15
Ru(100)					
	Ead/eV	-2.85	-1.86	-1.84	-1.67

BE_{diff}/eV	-	-0.87	-1.81	-1.16

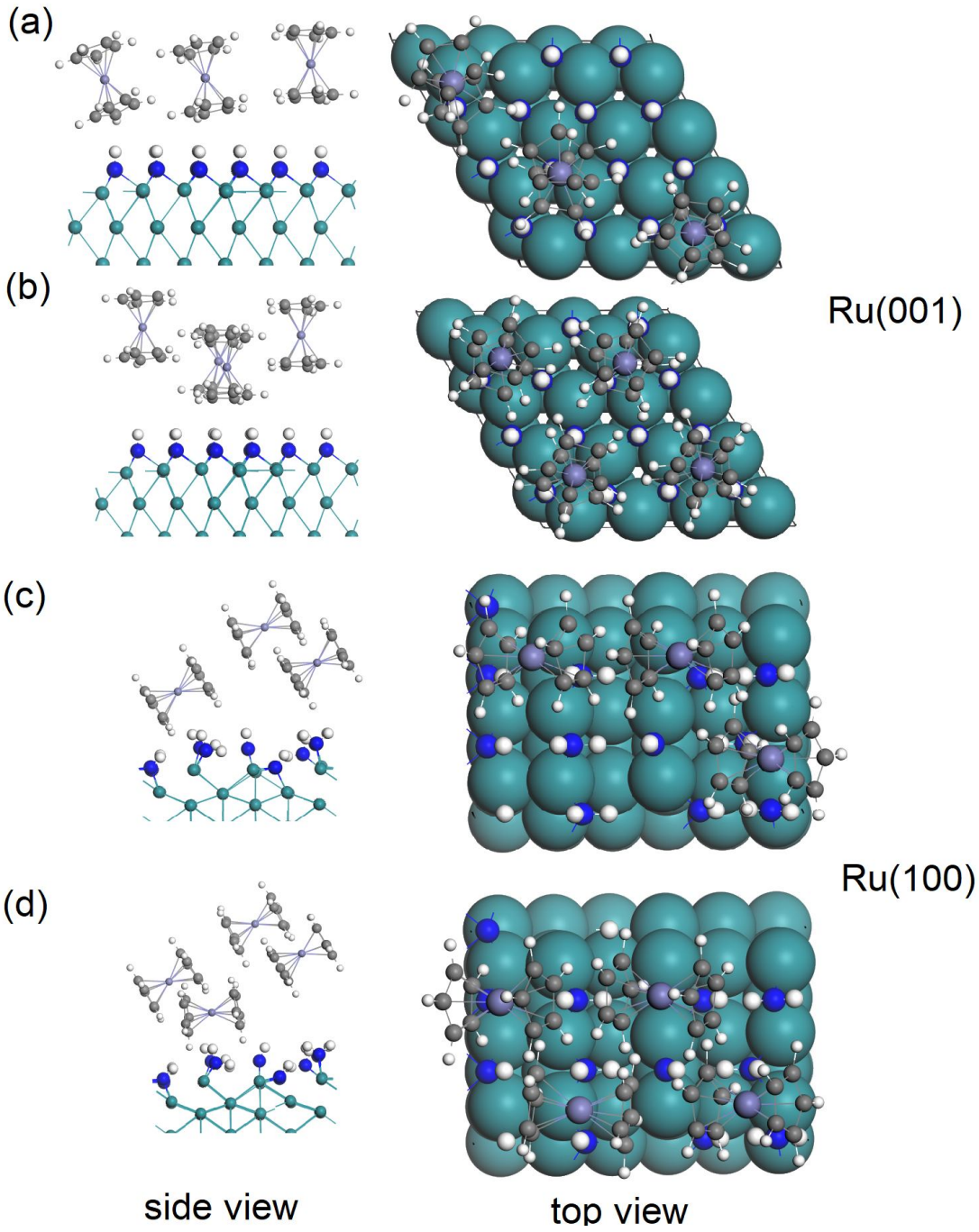

Figure 11. The side view and top view of $RuCp_2$ adsorption with (a) three $RuCp_2$ on Ru(001) surface, (b) four $RuCp_2$ on Ru(001) surface, (c) three $RuCp_2$ on Ru(100) surface, and four $RuCp_2$ on Ru(100) surface. The substrate Ru atoms are represented by green spheres and Ru atoms from

metal precursor are represented by purple spheres. Carbon, nitrogen and hydrogen atoms are represented by grey, blue and white colour, respectively.

The structures of adsorbing three $RuCp_2$ and four $RuCp^2$ on Ru(001) and Ru(100) surfaces are shown in Figure 11. Although the computed adsorption energy and binding energy difference are all negative, the final stable structures of these adsorbing $RuCp_2$ indicates that on Ru(001) surface, at most three $RuCp_2$ can be firmly adsorbed, while on Ru(100) surface, at most only two $RuCp_2$ can be firmly adsorbed. Thus, the determined maximum coverages of $RuCp_2$ on Ru(001) and Ru(100) surfaces are 2.54 $RuCp_2/nm^2$ and 2.02 $RuCp_2/nm^2$.

5. Conclusions

When depositing metals, non-oxidative reactant is preferred because O-source would cause contamination and oxidize metals. The ALD of Ru using metal precursor $RuCp_2$ and N-plasma have been investigated experimentally but the reaction mechanism is not well-understood. After the N-plasma step, the resulted metal surfaces will be NH_x-terminated. The nature and stability of NH_x-terminated metal surfaces are studied in our previous published work.[38] This work focuses on the reaction mechanism during the metal precursor pulse. The surface facets will result in different precursor adsorption orientation. $RuCp_2$ prefer upright position with one Cp ring in close contact with NH_x-terminated Ru(001) surface, while they are in horizontal position with both of the Cp rings anchored to zigzag channel on NH_x-terminated Ru(100) surface.

The Cp ligands are eliminated via hydrogen transfer step and desorb from surface by forming CpH. On Ru(001) surface, 1ML NH is preferred on Ru(001) surface at zero-K. With increasing temperature, NH will gradually desorb from surface, resulting in 0.89ML NH at ALD operating

condition. The hydrogen transfer reaction on Ru(001) surface is endothermic and the barrier is as high as 1.33eV and 1.51eV for 1ML NH termination and 0.89ML NH termination. Continuing decreasing NH coverage to extremely condition with 0.06ML NH (one NH on (4×4) supercell) leads to the similar positive reaction energy difference and at least moderate barrier. The nature of the NH_x-termination and the coverage of adsorbed precursor $RuCp_2$ have little effect on the elimination of the Cp ligand on Ru(001) surface. At most only one Cp ligand is eliminated, resulting RuCp fragment after metal precursor pulse at the coverage of 0.85 RuCp/nm^2.

On Ru(100) surface, two Cp ligands are eliminated via hydrogen transfer step. For single $RuCp_2$ adsorbed on NH_x-terminated Ru(100) surface, the barriers for the first and second hydrogen transfer are 2.01eV and 1.00eV, respectively. For two adsorbed $RuCp_2$ on NH_x-terminated Ru(100) surface, the barriers barely change, which are 2.02eV and 1.01eV for the first and second hydrogen transfer steps. In addition, there is H_2 formation during the reaction. This is important for the removal of surface NH_x species. At most two Ru atoms are deposited on Ru(100) surface, resulting a final coverage of 2.02 Ru/nm^2.

The metal precursor $RuCp_2$ has strong adsorption strength on NH_x-terminated Ru (001) and (100) surface. The computed activation barriers for the first hydrogen transfer are high on both (001) and (100) surface. This is irrespective of the coverage of surface adsorbed $RuCp_2$. The computed maximum coverages are 2.54 $RuCp_2$/nm^2 for Ru(001) and 2.02 $RuCp_2$/nm^2 for Ru(100). These adsorbing $RuCp_2$ or remaining RuCp fragment are eliminated by N_xH_y radicals from the N-plasma (NH_3 or mixture of N_2 and H_2) in the second half cycle.

Acknowledgements

We acknowledge generous support from Science Foundation Ireland (SFI) through the SFI-NSFC Partnership program, Grant Number 17/NSFC/5279, NITRALD and National Natural Science Foundation of China, Grant number 51861135105. Computing resources have been generously supported by Science Foundation Ireland at Tyndall and through the SFI/HEA-funded Irish Centre for High End Computing (www.ichec.ie).

References

1. Yim, S.-S.; Lee, D.-J.; Kim, K.-S.; Kim, S.-H.; Yoon, T.-S.; Kim, K.-B., Nucleation kinetics of Ru on silicon oxide and silicon nitride surfaces deposited by atomic layer deposition. *J. Appl. Phys.* **2008,** *103*, 113509.
2. Kim, S.; Duquette, D. J., Effect of chemical composition on adhesion of directly electrodeposited copper film on TiN. *J. Electrochem. Soc.* **2006,** *153*, C417.
3. Johnson, R. W.; Hultqvist, A.; Bent, S. F., A brief review of atomic layer deposition: from fundamentals to applications. *Mater. Today* **2014,** *17*, 236-246.
4. Kaloyeros, A. E.; Pan, Y.; Goff, J.; Arkles, B., Review—Cobalt Thin Films: Trends in Processing Technologies and Emerging Applications. *ECS J. Solid State Sci.* **2019,** *8*, P119-P152.
5. Josell, D.; Wheeler, D.; Witt, C.; Moffat, T. P., Seedless superfill: Copper electrodeposition in trenches with ruthenium barriers. *Electrochem. Solid State Lett.* **2003,** *6*, C143.
6. Han, J. H.; Lee, S. W.; Choi, G.-J.; Lee, S. Y.; Hwang, C. S.; Dussarrat, C.; Gatineau, J., Chemical vapor deposition of Ru thin films with an enhanced morphology, thermal stability, and electrical properties using a RuO4 precursor. *Chem. Mater.* **2009,** *21*, 207-209.
7. George, S. M., Atomic layer deposition: an overview. *Chem. Rev.* **2009,** *110*, 111-131.
8. Profijt, H.; Potts, S.; Van de Sanden, M.; Kessels, W., Plasma-assisted atomic layer deposition: basics, opportunities, and challenges. *J. Vac. Sci. Technol. A* **2011,** *29*, 050801.
9. Miikkulainen, V.; Leskelä, M.; Ritala, M.; Puurunen, R. L., Crystallinity of inorganic films grown by atomic layer deposition: Overview and general trends. *J. Appl. Phys.* **2013,** *113*, 2.

10. Kwon, S.-H.; Kwon, O.-K.; Kim, J.-H.; Jeong, S.-J.; Kim, S.-W.; Kang, S.-W., Improvement of the morphological stability by stacking RuO2 on ru thin films with atomic layer deposition. *J. Electrochem. Soc.* **2007,** *154*, H773-H777.

11. Ramos, K. B.; Saly, M. J.; Chabal, Y. J., Precursor design and reaction mechanisms for the atomic layer deposition of metal films. *Coordin. Chem. Rev.* **2013,** *257*, 3271-3281.

12. Cwik, S.; Woods, K. N.; Saly, M. J.; Knisley, T. J.; Winter, C. H., Thermal atomic layer deposition of ruthenium metal thin films using nonoxidative coreactants. *J. Vac. Sci. Technol. A* **2020,** *38*, 012402.

13. Swerts, J.; Delabie, A.; Salimullah, M.; Popovici, M.; Kim, M.-S.; Schaekers, M.; Van Elshocht, S., Impact of the plasma ambient and the ruthenium precursor on the growth of ruthenium films by plasma enhanced atomic layer deposition. *Electrochem. Solid-State Lett.* **2012,** *1*, P19-P21.

14. Kwon, O.-K.; Kwon, S.-H.; Park, H.-S.; Kang, S.-W., Plasma-enhanced atomic layer deposition of ruthenium thin films. *Electrochem. Solid State Lett.* **2004,** *7*, C46.

15. Sari, W.; Eom, T.-K.; Kim, S.-H.; Kim, H., Plasma Enhanced Atomic Layer Deposition of Ruthenium Thin Films Using Isopropylmethylbenzene-Cyclohexadiene-Ruthenium and NH3 Plasma. *J. Electrochem. Soc.* **2010,** *158*, D42.

16. Park, S.-J.; Kim, W.-H.; Maeng, W.; Kim, H., Thermal and plasma enhanced atomic layer deposition ruthenium and electrical characterization as a metal electrode. *Microelectron. Eng.* **2008,** *85*, 39-44.

17. Hämäläinen, J.; Ritala, M.; Leskelä, M., Atomic Layer Deposition of Noble Metals and Their Oxides. *Chem. Mater.* **2014,** *26*, 786-801.

18. Park, S.-J.; Kim, W.-H.; Maeng, W.; Yang, Y.; Park, C.; Kim, H.; Lee, K.-N.; Jung, S.-W.; Seong, W., Effect oxygen exposure on the quality of atomic layer deposition of ruthenium from bis (cyclopentadienyl) ruthenium and oxygen. *Thin Solid Films* **2008,** *516*, 7345-7349.

19. Leick, N.; Verkuijlen, R.; Lamagna, L.; Langereis, E.; Rushworth, S.; Roozeboom, F.; Van de Sanden, M.; Kessels, W., Atomic layer deposition of Ru from CpRu (CO) 2 Et using O 2 gas and O 2 plasma. *J. Vac. Sci. Technol. A* **2011,** *29*, 021016.

20. Lee, S.-J.; Kim, S.-H., Effects of Annealing on the Properties of Atomic Layer Deposited Ru Thin Films Deposited by NH_3 and H_2 as Reactants. *Thin Solid Films* **2016,** *612*, 122-127.

21. Lee, S.-J.; Kim, S.-H.; Saito, M.; Suzuki, K.; Nabeya, S.; Lee, J.; Kim, S.; Yeom, S.; Lee, D.-J., Plasma-Free Atomic Layer Deposition of Ru Thin Films Using H_2 Molecules as A Nonoxidizing Reactant. *J. Vac. Sci. Technol. A* **2016,** *34*, 031509.

22. Gakis, G. P.; Vergnes, H.; Cristiano, F.; Tison, Y.; Vahlas, C.; Caussat, B.; Boudouvis, A. G.; Scheid, E., In situ N2-NH3 plasma pre-treatment of silicon substrate enhances the initial growth and restricts the substrate oxidation during alumina ALD. *J. Appl. Phys* **2019,** *126*, 125305.

23. Minjauw, M. M.; Dendooven, J.; Capon, B.; Schaekers, M.; Detavernier, C., Near room temperature plasma enhanced atomic layer deposition of ruthenium using the RuO 4-precursor and H 2-plasma. *J. Mater. Chem. C* **2015,** *3*, 4848-4851.

24. Musschoot, J.; Xie, Q.; Deduytsche, D.; De Keyser, K.; Longrie, D.; Haemers, J.; Van den Berghe, S.; Van Meirhaeghe, R.; D'Haen, J.; Detavernier, C., Texture of atomic layer deposited ruthenium. *Microelectron. Eng.* **2010,** *87*, 1879-1883.

25. Elliott, S. D., Atomic-scale simulation of ALD chemistry. *Semicond. Sci. Tech.* **2012,** *27*, 074008.

26. Phung, Q. M.; Pourtois, G.; Swerts, J.; Pierloot, K.; Delabie, A., Atomic Layer Deposition of Ruthenium on Ruthenium Surfaces: A Theoretical Study. *J. Phys. Chem. C* **2015,** *119*, 6592-6603.

27. Elliott, S. D.; Dey, G.; Maimaiti, Y., Classification of processes for the atomic layer deposition of metals based on mechanistic information from density functional theory calculations. *J. Chem. Phys.* **2017,** *146*, 052822.

28. Phung, Q. M.; Vancoillie, S.; Pourtois, G.; Swerts, J.; Pierloot, K.; Delabie, A., Atomic Layer Deposition of Ruthenium on a Titanium Nitride Surface: A Density Functional Theory Study. *J. Phys. Chem. C* **2013,** *117*, 19442-19453.

29. Fang, G.; Xu, L.; Cao, Y.; Li, A., Theoretical design and computational screening of precursors for atomic layer deposition. *Coordin. Chem. Rev.* **2016,** *322*, 94-103.

30. Holme, T. P.; Prinz, F. B., Atomic Layer Deposition and Chemical Vapor Deposition Precursor Selection Method Application to Strontium and Barium Precursors. *J. Phys. Chem. A* **2007,** *111*, 8147-8151.

31. Puurunen, R. L., Surface chemistry of atomic layer deposition: A case study for the trimethylaluminum/water process. *J. Appl. Phys* **2005,** *97*, 9.

32. Elliott, S.; Scarel, G.; Wiemer, C.; Fanciulli, M.; Pavia, G., Ozone-Based Atomic Layer Deposition of Alumina from TMA: Growth, Morphology, and Reaction Mechanism. *Chem. Mater.* **2006,** *18*, 3764-3773.

33. Langereis, E.; Bouman, M.; Keijmel, J.; Heil, S.; Van de Sanden, M.; Kessels, W., Plasma-assisted ALD of Al2O3 at low temperatures: reaction mechanisms and material properties. *ECS Trans.* **2008,** *16*, 247-255.

34. Rai, V. R.; Vandalon, V.; Agarwal, S., Surface reaction mechanisms during ozone and oxygen plasma assisted atomic layer deposition of aluminum oxide. *Langmuir* **2010,** *26*, 13732-13735.

35. Weckman, T.; Laasonen, K., First principles study of the atomic layer deposition of alumina by TMA–H 2 O-process. *Phys. Chem. Chem. Phys.* **2015,** *17*, 17322-17334.

36. Kwon, D. S.; An, C. H.; Kim, S. H.; Kim, D. G.; Lim, J.; Jeon, W.; Hwang, C. S., Atomic layer deposition of Ru thin films using (2, 4-dimethyloxopentadienyl)(ethylcyclopentadienyl) Ru and the effect of ammonia treatment during the deposition. *J. Mater. Chem. C* **2020**.

37. Liu, J.; Lu, H.; Zhang, D. W.; Nolan, M., Reaction Mechanism of the Metal Precursor Pulse in Plasma-Enhanced Atomic Layer Deposition of Cobalt and the Role of Surface Facets. *J. Phys. Chem. C* **2020,** *124*, 11990-12000.

38. Liu, J.; Nolan, M., Coverage and Stability of NHx-Terminated Cobalt and Ruthenium Surfaces: A First-Principles Investigation. *J. Phys. Chem. C* **2019,** *123*, 25166-25175.

39. Kresse, G.; Joubert, D., From ultrasoft pseudopotentials to the projector augmented-wave method. *Phys. Rev. B* **1999,** *59*, 1758.

40. Perdew, J. P.; Chevary, J. A.; Vosko, S. H.; Jackson, K. A.; Pederson, M. R.; Singh, D. J.; Fiolhais, C., Atoms, molecules, solids, and surfaces: Applications of the generalized gradient approximation for exchange and correlation. *Phys. Rev. B* **1992,** *46*, 6671.

41. Perdew, J. P.; Burke, K.; Ernzerhof, M., Generalized gradient approximation made simple. *Phys. Rev. Lett.* **1996,** *77*, 3865.

42. Monkhorst, H. J.; Pack, J. D., Special points for Brillouin-zone integrations. *Phys. Rev. B* **1976,** *13*, 5188.

43. Maimaiti, Y.; Elliott, S. D., Precursor Adsorption on Copper Surfaces as the First Step during the Deposition of Copper: A Density Functional Study with van der Waals Correction. *J. Phys. Chem. C* **2015,** *119*, 9375-9385.

44. Henkelman, G.; Uberuaga, B. P.; Jónsson, H., A climbing image nudged elastic band method for finding saddle points and minimum energy paths. *J. Chem. Phys.* **2000,** *113*, 9901-9904.

45. Cluff, K. J.; Blümel, J., Adsorption of Metallocenes on Silica. *Chem. Eur. J* **2016,** *22*, 16562-16575.

46. Aaltonen, T.; Alén, P.; Ritala, M.; Leskelä, M., Ruthenium thin films grown by atomic layer deposition. *Chem. Vap. Depos.* **2003,** *9*, 45-49.

47. Kwon, S.-H.; Kwon, O.-K.; Min, J.-S.; Kang, S.-W., Plasma-enhanced atomic layer deposition of Ru–TiN thin films for copper diffusion barrier metals. *J. Electrochem. Soc.* **2006,** *153*, G578.